

The Broad Wing of [O III] $\lambda 5007$ Emission Line in Active Galactic Nuclei

Zhixin Peng^{1,2}, Yanmei Chen^{1,2}, Qiusheng Gu^{1,2} and Kai Zhang³

¹ School of Astronomy and Space Science, Nanjing University, Nanjing 210093, P. R. China;
zxpeng@nju.edu.cn

² Key Laboratory of Modern Astronomy and Astrophysics (Nanjing University), Ministry of Education, Nanjing 210093, China

³ Key Laboratory for Research in Galaxies and Cosmology, Shanghai Astronomical Observatory, Chinese Academy of Sciences, 80 Nandan Road, Shanghai 200030, P. R. China

Received [year] [month] [day]; accepted [year] [month] [day]

Abstract We use a type 2 AGN sample from SDSS DR7 in which the [O III] $\lambda 5007$ emission line can be modeled by two Gaussian components, a broad wing plus a narrow core, to investigate the origin of the broad wing and the connection between the velocity shift of the broad wing and the physical parameters of active galactic nuclei (AGNs) as well as their host galaxies. We find that the flux of the wing components is roughly equal to that of the core components in statistic. However, the velocity shift of the wing component has only weak, if any, correlations with the physical properties of AGNs and the host galaxies such as bolometric luminosity, the Eddington ratio, the mass of supermassive black holes, $D4000$, $H\delta_A$ or stellar mass. Comparing the velocity shift from our type 2 AGN sample to that from type 1 sample in Zhang et al. (2011), we suggest the [O III] broad wing originates from outflow.

Key words: galaxies: active – galaxies: Seyfert – quasars: emission lines

1 INTRODUCTION

Active galactic nuclei (AGNs) feedback now appears as a crucial process in galaxy formation and evolution. It is well-known that the tight correlation between nuclear black hole mass (M_{BH}) and bulge stellar velocity dispersion (i.e., the $M_{\text{BH}} - \sigma_*$ relation; Ferrarese & Merritt 2000; Gebhardt et al. 2000; Tremaine et al. 2002) is compelling evidence for a close connection between the evolution of supermassive black holes and their host galaxies. AGN feedback is the most likely explanation for this relation (e.g., Silk & Rees 1998; Fabian 1999). Hopkins et al. (2006) also indicate the importance of feedback in the evolutionary model for starbursts, AGN activity and spheroidal galaxies. This feedback can terminate star formation in the host galaxy and cease gas accretion onto the nuclear black hole, with the form of radiation, winds, jets and outflows.

The various emission lines from narrow-line regions (NLRs) of AGN are ideally suited to study the central regions of AGNs, as well as the interaction between the central engine and its host galaxy. Unlike the broad-line regions (BLRs), the NLR is spatially resolvable, at least for nearby galaxies. It is generally believed that the narrow emission lines are produced by clouds illuminated by the central AGN, and the kinematics of the NLR clouds are mainly dominated by the gravitational potential of the bulge (e.g., Whittle 1992; Nelson & Whittle 1996). Since the NLR connects to various factors such as

the energy input from the central engine, the structure of AGN, radio jets, and star formation etc, it accesses a number of key questions of AGN phenomenon.

[O III] $\lambda\lambda 4959, 5007$ emission lines are commonly used to study the properties of NLRs. It is usually the strongest narrow line in AGNs at optical band and cleanly isolated from other emission and absorption features in the optical spectrum. The line profile of [O III] doublets in low-redshift AGNs is usually asymmetric. In most case, there is a sharper fall-off to the red than to the blue, and the redshift of [O III] is negative compared to the system velocity derived from different indicators, such as the low-ionization lines ([N II], [S II]), or stellar absorption lines (Heckman et al. 1981 and consequent researches). This asymmetry feature of [O III] line has been suggested as an indicator of outflows in Seyfert 1s and 2s (Heckman et al. 1981; Whittle et al. 1988; Colbert et al. 1996; Crenshaw et al. 2010), Narrow Line Seyfert 1 galaxies (Bian et al. 2005; Komossa et al. 2008), type 1 quasars (Heckman et al. 1984; Boroson 2005) and narrow line radio galaxies (Holt et al. 2008).

It is now believed that a broad blue wing in addition to the main narrow component is ubiquitous in [O III] emission. Many previous studies suggest this blue wing is contributed by AGN outflows, they also attempt to correlate the parameters of lines, such as the [O III] blueshift or/and the [O III] line width, with the physical properties of AGNs (Zamanov et al. 2002; Aoki et al. 2005; Boroson 2005; Bian et al. 2005; Komossa et al. 2008). Based on homogeneous samples of radio-quiet Seyfert 1 galaxies and QSOs selected from SDSS, Zhang et al. (2011) find that the blueshift of [O III] has only weak correlations with fundamental AGN parameters, such as the nuclear continuum luminosity at 5100Å (L_{5100}), black hole mass (M_{BH}), and the Eddington ratio ($L_{\text{bol}}/L_{\text{Edd}}$). Alexander & Hickox (2012) mentioned that in statistics, the width and luminosity of the blue wing increase with [O III] luminosity, but independent of radio loudness, indicating the outflows are driven by AGN radiation rather than relativistic jets. Zhang et al. (2008) found that Seyfert 1s have lower [N II]/H α ratios than Seyfert 2s and the location of Seyfert 1s on the BPT diagram varies with extinction of broad lines, suggesting that the inner dense NLR is obscured by dusty torus. The inner dense NLR might be the place where the [O III] blue wing originates (Zhang et al. 2013). Stern & Laor (2013) revisit the location of type 1 and type 2 AGNs on the BPT diagrams, finding similar result as Zhang et al. (2008)—type 1 AGNs are offset to lower [S II]/H α and [N II]/H α ratios. However, they conclude that this offset between type 1 and type 2 AGNs is a selection effect rather than dust extinction.

In this paper, we will explore the asymmetric behavior of [O III] $\lambda\lambda 4959, 5007$ lines in more detail, studying the origin of [O III] asymmetry. In Section 2, we describe the sample selection and data analysis. We show the results in Section 3. In Section 4, the origin of the broad wing is discussed. Our conclusions are given in Section 5. Throughout this paper, a cosmology with $H_0 = 70 \text{ km s}^{-1} \text{ Mpc}^{-1}$, $\Omega_m = 0.3$, and $\Omega_\Lambda = 0.7$ is adopted.

2 SAMPLE AND DATA ANALYSIS

2.1 The Sample

We begin with the galaxy sample of SDSS (York et al. 2000) seventh data release (DR7; Abazajian et al. 2009) and select type 2 active galaxies based on the widely used BPT diagram (Baldwin et al. 1981). The SDSS DR7 spectroscopic galaxy catalog contains $\sim 930,000$ spectra taken through 3'' diameter fiber in the primary redshift range $0 \lesssim z \lesssim 0.3$. Flux and equivalent width (EQW) of narrow emission lines (e.g., H α , [N II] $\lambda 6583$, [O III] $\lambda 5007$, H β) as well as line indices D4000, H δ_A and stellar mass have been publicly available since 2008 in the MPA/JHU catalog¹.

The criteria used to select the parent type 2 AGN sample used in our analysis are the following:

1. Redshift between $0.01 \leq z \leq 0.3$ and specPrimary = 1. The lower redshift limit of 0.01 is applied to avoid the influence of peculiar velocity. SpecPrimary = 1 deletes repeat observations from the sample.

¹ The raw data files of this catalogue can be downloaded from <http://www.mpa-garching.mpg.de/SDSS/DR7/>

2. $\log([\text{O III}]/\text{H}\beta) > 0.61/[\log([\text{N II}]/\text{H}\alpha) - 0.47] + 1.19$ (the solid curve in Figure 2 from [Kauffmann et al. 2003](#)), or $\log([\text{N II}]/\text{H}\alpha) \geq 0.47$. For those objects with $\text{H}\alpha$, $[\text{N II}]$, $[\text{O III}]$, and $\text{H}\beta$ emission lines detected with signal-to-noise ratio (S/N) > 3 , we separate type 2 AGNs from other sources using the emission line ratio diagnostics.
3. The EQW of $[\text{O III}] \lambda 5007$ emission line is smaller than -5 (negative EQW means emission) and the median S/N per pixel in the rest-frame wavelength range $4880\text{--}4920\text{\AA}$ and $5030\text{--}5070\text{\AA}$ (the continuum around $[\text{O III}]$) greater than 15. The high spectral quality requirement around $[\text{O III}]$ region ensures reliable analysis of the line profile.

We refer to this sample hereafter as “parent sample”. It contains 9,389 type 2 AGNs. Other parameters which would be used in this paper like stellar mass (M_*), absorption line indices (D4000 and $\text{H}\delta_{\text{A}}$) and stellar velocity dispersion (V_{disp}) are also provided in the MPA/JHU catalog.

2.2 Fitting the Stellar Continuum

The aim of this study is to use the $[\text{O III}]$ emission line to probe outflows in the NLR. In order to get pure emission line spectra, we need to model the stellar continuum of each galaxy. As described in [Tremonti et al. \(2004\)](#) and [Brinchmann et al. \(2004\)](#), the continua and absorption lines of each galaxy are fitted by a stellar population. The basic assumption is that any galaxy star formation history can be approximated by a sum of discrete bursts. The library of template spectra is composed of single stellar population (SSP) models generated using a preliminary version of the population synthesis code of [Charlot & Bruzual \(2013\)](#), including models of 10 different ages (0.005, 0.025, 0.1, 0.2, 0.6, 0.9, 1.4, 2.5, 5, and 10 Gyr) and four metallicities (0.004, 0.008, 0.017, and 0.04). For each metallicity, the ten template spectra with different ages are convolved to the measured stellar velocity dispersion of the SDSS galaxy, and the best-fitting model spectrum is constructed from a non-negative linear combination of the ten template spectra, with dust attenuation modeled as an additional free parameter. The metallicity which yields the minimum χ^2 is selected as the final best fit. The fitting results can be found on the SDSS-MPA Web site.

2.3 Fitting the Emission Lines

After subtracting the stellar continuum model, we use the following simple method to fit $[\text{O III}] \lambda\lambda 4959, 5007$ emission lines. First, we use only one Gaussian to model each $[\text{O III}]$ line (hereafter the single-Gaussian model), $[\text{O III}] \lambda 4959$ is forced to have the same profile and shift as $[\text{O III}] \lambda 5007$. We use the galaxy redshift from SDSS pipeline to define rest frame. We also decompose each $[\text{O III}]$ line into two Gaussians (hereafter the double-Gaussian model), a narrow core ($[\text{O III}]_{4959}^{\text{NC}}$ and $[\text{O III}]_{5007}^{\text{NC}}$) and a broad wing ($[\text{O III}]_{4959}^{\text{BW}}$ and $[\text{O III}]_{5007}^{\text{BW}}$). Each component of $[\text{O III}] \lambda 4959$ is tied to the relevant component of $[\text{O III}] \lambda 5007$ in the same way as that in the single-Gaussian model. The line center is limited in the range of $4980\text{--}5050 \text{\AA}$. We compare the reduced χ^2 of the single-Gaussian and double-Gaussian model, and use the F-test ([Lupton, 1993](#), chap. 12.1) to calculate how significantly the fit is improved by the double-Gaussian model. Figure 1 shows the probability level (σ_{P}) that the double-Gaussian model can improve the fit of emission lines, as a function of the improvement of χ^2 , which is defined as $(\chi_{\text{one}}^2 - \chi_{\text{two}}^2)/\chi_{\text{one}}^2$. χ_{one}^2 is the reduced χ^2 of the single-Gaussian model and χ_{two}^2 is the reduced χ^2 of the double Gaussian model. We select the 1,630 sources up the horizontal dashed line as our sample for studying outflow. These galaxies require two Gaussians at a significance greater than 8σ , with χ^2 improvement greater than $\sim 65\%$.

3 RESULTS

With the double-Gaussian model fitting of the 1,630 sources in the sample, we find the velocity shifts of the core component, $V_{\text{off}}^{\text{core}} = (\lambda_{\text{core}} - \lambda_0)/\lambda_0 \times c$, has a Gaussian distribution over a range of $-200 \sim 200 \text{ km s}^{-1}$, with a median value at 8 km s^{-1} and 68% of the total probability distribution

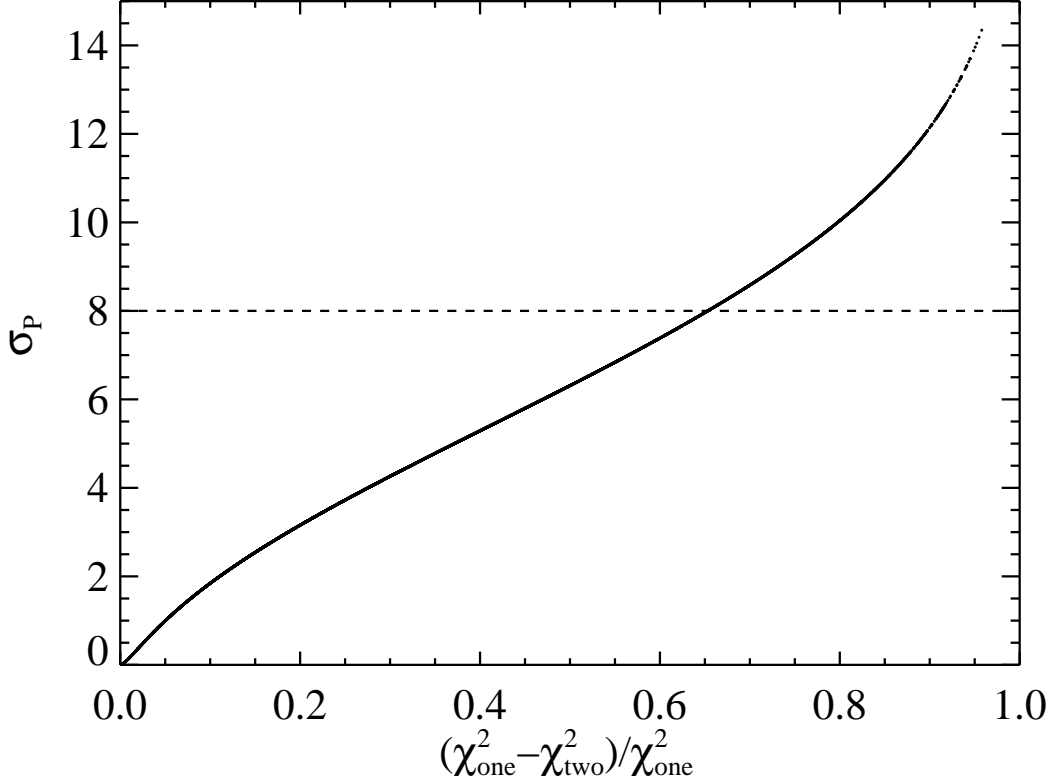


Fig. 1 The probability level (σ_P) of the improvement of the fit of emission lines. We select the sources up the horizontal dashed line as our sample.

distributed over the range $-37 \sim 53 \text{ km s}^{-1}$. Here λ_{core} is the central wavelength of the core component, $\lambda_0 = 5006.84$ is the rest-frame line center of [O III] in air, c is the speed of light. The distribution of velocity shifts of the wing component is highly deviated from Gaussian with a median shift of -72 km s^{-1} . We note that the pipeline redshift is determined from both the emission lines and the continuum. If the emission lines are blueshifted, then the pipeline redshifts tend to be underestimated. Here we re-determine the system redshift from the continuum and absorption lines: starting from the stellar continuum model given in section 2.2, we iteratively increase/decrease the system velocity by 5 km s^{-1} and re-calculate a χ^2 value, the absorption line redshift is determined by the case with the lowest χ^2 value. In the following section, we use this absorption line redshift to define rest-frame. Figure 2 shows one example of the two component fit, the black is the observed emission line spectrum, the broad wing and the narrow core are shown in blue and red, respectively, the best fit model is over-plotted in green.

3.1 Correlation between Wing and Core Flux

In Figure 3, we show the correlation between the fluxes of the wing (F_{wing}) and core (F_{core}) of [O III] $\lambda 5007$ emission line for both type 1 (red dots) and type 2 (black dots) AGNs sample. The type 1 AGN sample contains 383 objects from Zhang et al. (2011) with a redshift range of $0.01 \leq z \leq 0.3$. The green line, $\log F_{\text{wing}} = (0.792 \pm 0.070) \log F_{\text{core}} - (3.112 \pm 1.016)$, is the best linear least-square fit for type 1 AGNs with the Spearman rank-order correlation coefficient (r_S) of 0.663, while the blue line, $\log F_{\text{wing}} = (0.724 \pm 0.035) \log F_{\text{core}} - (3.964 \pm 0.496)$, is the fit for type 2 AGNs, with $r_S = 0.649$.

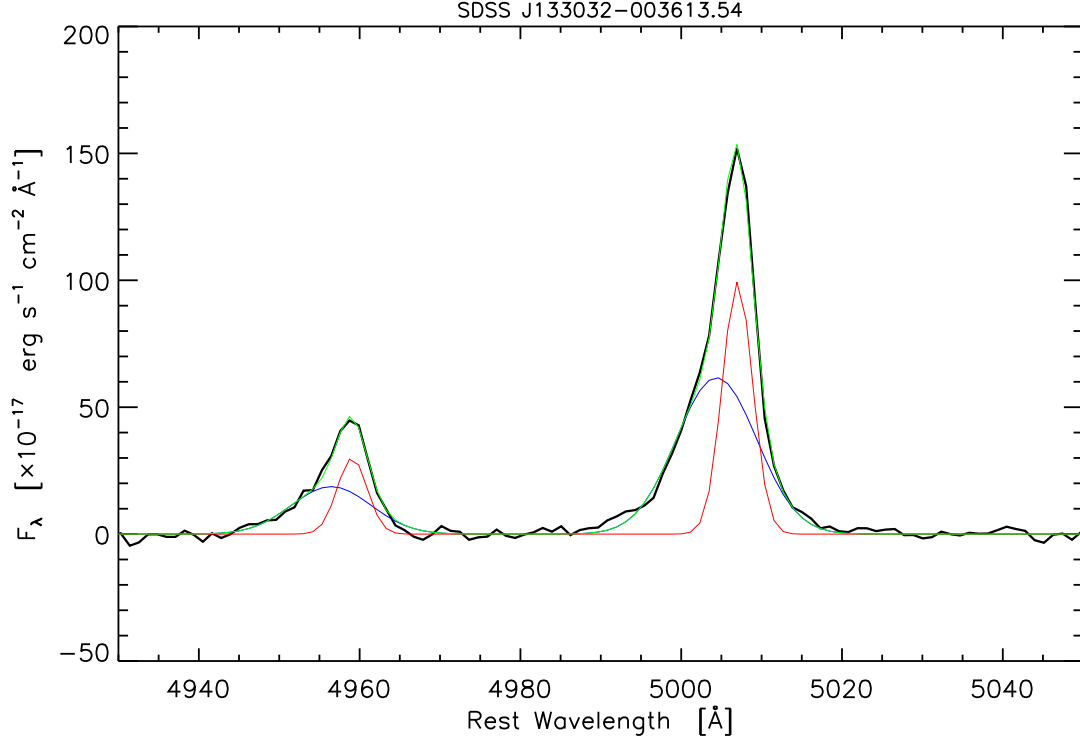


Fig. 2 An example of double Gaussian fit. For each [O III] emission line, two Gaussian components are used. The red represents the core component, and the blue one is the underlying broad wing. The best fit model is shown in green.

Zhang et al. (2011) found that on average, the core component comprise 54% of the total emission, which is consistent with a 52% contribution of the core component in our type 2 sample. The detailed explanation of this strong correlation between the fluxes of core and wing components in both type 1 and type 2 AGNs is beyond the scope of the current paper, we will build a model to understand this correlation in a following paper.

3.2 How $V_{\text{off}}^{\text{wing}}$ Depends on the Properties of Galaxies

Since the blue asymmetry of [O III] profile generally suggests the exist of outflow, we explore whether the shift of the broad wing is connected with the strength of AGN activity and star formation which are the primary driver of the outflow. We estimate the bolometric luminosity of the AGN as $L_{\text{bol}} \approx 600 L_{[\text{O III}]}$ (Kauffmann & Heckman 2009). $L_{[\text{O III}]}$ is the total luminosity of wing and core with dust extinction from Balmer decrement, and the correlation in this section is independent on which [O III] luminosity we use, $L_{[\text{O III}]}^{\text{wing}}$, $L_{[\text{O III}]}^{\text{core}}$, or $L_{[\text{O III}]}^{\text{wing}} + L_{[\text{O III}]}^{\text{core}}$. The Eddington ratio is defined as $\lambda = L_{\text{bol}}/L_{\text{Edd}}$, where $L_{\text{Edd}} \equiv 1.26 \times 10^{38} (M_{\text{BH}}/M_{\odot}) \text{ erg s}^{-1}$. The mass of the central black hole is estimated from the famous $M_{\text{BH}} - \sigma_*$ relation (Ferrarese & Merritt 2000; Gebhardt et al. 2000) of the form $\log(M_{\text{BH}}/M_{\odot}) = 8.13 + 4.02 \log(\sigma_*/200)$ (Tremaine et al. 2002), where σ_* is the stellar velocity dispersion.

Figure 4 shows the velocity shift of wing component ($V_{\text{off}}^{\text{wing}}$) as a function of L_{bol} , λ , mass of supermassive black holes (M_{BH}), D4000, $\text{H}\delta_{\text{A}}$ and stellar mass (M_*). The stellar mass (M_*) and absorption line indices (D4000 and $\text{H}\delta_{\text{A}}$) are provided in MPA/JHU catalog. The red lines are the median.

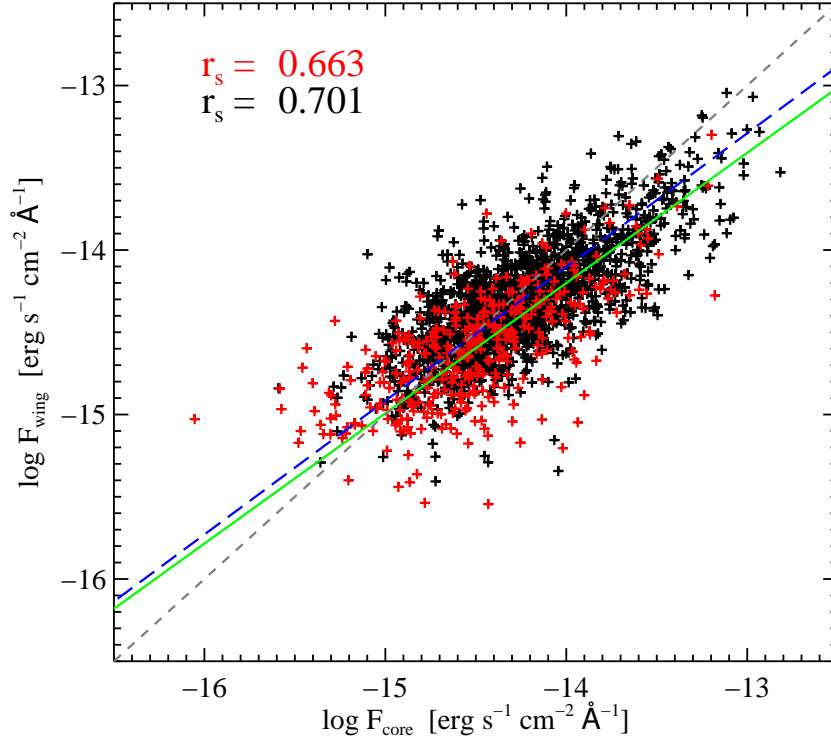


Fig. 3 Correlation between the fluxes of broad wing and narrow core of [O III] $\lambda 5007$ emission line in type 1 (*red*) and type 2 (*black*) AGNs. The Spearman rank-order correlation coefficients (r_s) are 0.663 (0.649) for type 1 (type 2) AGNs. The best linear Least-squares approximation is shown, green line for type 1s, and blue long dash line for type 2s. The gray dash line is the $x = y$ line.

Table 1 Correlation Results between $V_{\text{off}}^{\text{wing}}$ and Galaxy Properties

correlation	L_{bol}	λ	M_{BH}	D4000	H δ_A	M_*
r_S	-0.184	0.010	-0.083	0.097	-0.204	-0.083
P_{null}	8.9e-13	6.8e-1	1.3e-3	1.9e-4	1.9e-15	1.3e-3

The correlation results are listed in Table 1, where r_S is the Spearman rank-order correlation coefficient and P_{null} is the probability for the null hypothesis of no correlation. The high significant of P_{null} is due to the large number of sources in our sample. In summary, we have not found any distinct correlation between $V_{\text{off}}^{\text{wing}}$ and galaxy properties. Outflow is driven by both AGN and star formation activity. However, the contribution of AGN and star formation activity to the outflow varies from object to object. This leads to a lack of correlation in Figure 4. The result is consistent with that in Komossa et al. (2008) and Zhang et al. (2011).

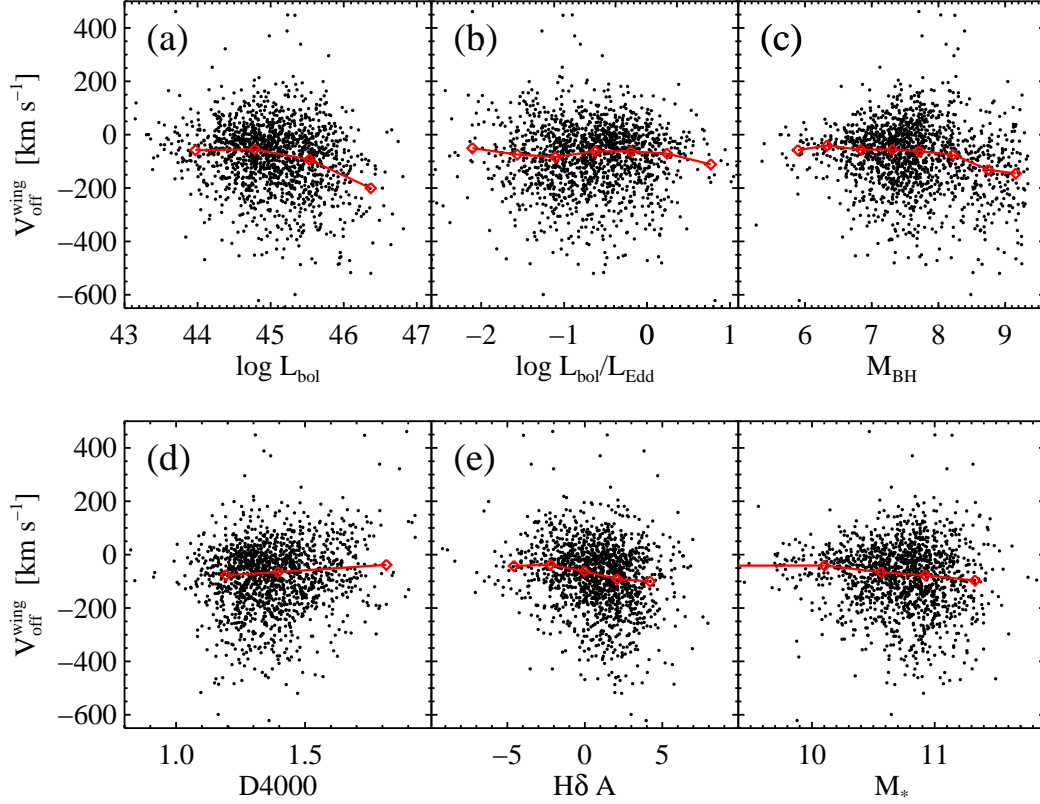


Fig. 4 Velocity shifts of the wing component relative to the system velocity $V_{\text{off}}^{\text{wing}}$ versus L_{bol} , λ , M_{BH} , $D4000$, $H\delta_A$ and M_* . Diamonds are the position of median value in each bin.

3.3 Comparison with Type 1 AGNs

In the standard AGN unified scheme, type 1 and type 2 AGNs are intrinsically the same objects. As a result of obscuration of torus, the radiation originated from the accretion disc will push materials out mostly along the rotation axis of the accretion disc. If the blue wing of [O III] is triggered by outflows, we should observe a faster velocity in type 1 than in type 2 AGNs due to the inclination effect. In order to avoid any evolution effect and make a fair comparison between type 1 and type 2 AGNs, we construct twin subsamples from the type 1 (Zhang et al. 2011) and type 2 AGNs by matching their redshift with a tolerance of $\Delta z = 0.004$, namely, the type 1 and type 2 subsamples have exactly the same redshift distribution. See the histograms in Figure 5. The black, blue and red lines show the redshift distributions for type 1, type 2 AGNs, and the matched twin sample, respectively. Through this redshift match, each subsample contains 264 objects. Figure 6 ~ 7 show the distributions of velocity offset and line width of the [O III] wing and core components for the twin subsamples, and the median values are shown by vertical dashed lines, black for type 1 and blue for type 2 AGNs.

In Fig. 6, we show the distributions of the velocity offset relative to the system velocity, $V_{\text{off}}^{\text{core}}$ and $V_{\text{off}}^{\text{wing}}$. The system velocity is derived from [S II] emission line for type 1 sample and from stellar absorption lines for type 2 sample. The median values of $V_{\text{off}}^{\text{core}}$ are -11 km s^{-1} , and 6 km s^{-1} for type 1 and type 2 subsamples, and the median values of $V_{\text{off}}^{\text{wing}}$ are -162 km s^{-1} , and -97 km s^{-1} for type 1 and type 2 subsamples, respectively.

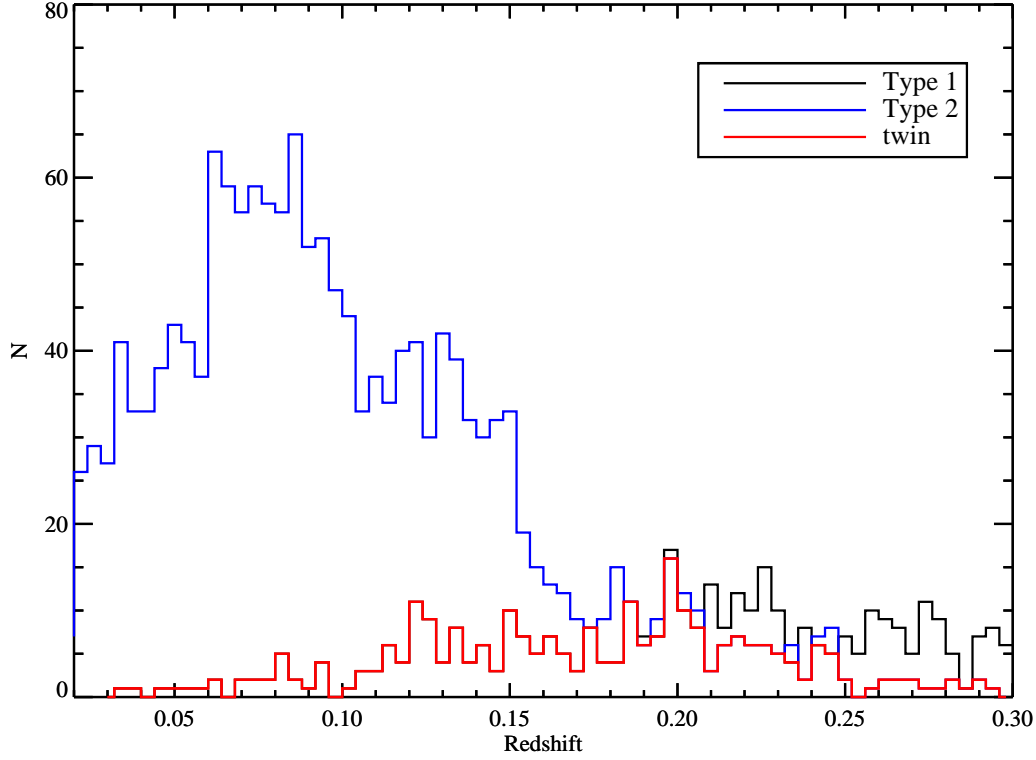


Fig. 5 Redshift distribution of type 1 (*black*) and type 2 (*blue*) AGN sample. The red histogram shows the redshift distribution of the twin sample.

In Fig. 7, we show the distributions of line width of wing (σ_{wing}) and core (σ_{core}) components. The median values of σ_{core} are 138 km s^{-1} and 131 km s^{-1} for type 1 and type 2 subsamples, and the median values of σ_{wing} are 393 km s^{-1} and 370 km s^{-1} for type 1 and type 2 subsamples, respectively. Basically, there is no difference in σ_{core} and σ_{wing} between type 1 and type 2 AGNs.

4 ORIGIN OF THE BROAD WING

In this section, we discuss the origin of the broad wing of [O III] $\lambda\lambda 4959, 5007$, including its location and physical mechanism, based on the observational results in section 3.

1. **Location.** We derive black hole mass (M_{BH}) from the $M_{\text{BH}} - \sigma_*$ relation. At the same time, if we assume the region which generates the wing component is still dominated by the potential of central super-massive black hole, we can estimate the location of the region (R_{wing}) where the wing comes from as $R_{\text{wing}} = G \frac{M_{\text{BH}}}{f \Delta V^2}$, f is the scaling factor with a value of 3.85 (Collin et al. 2006), ΔV is the emission line width, we set $\Delta V = \sigma_{\text{wing}}$, $G = 6.67384 \times 10^{-11} \text{ m}^3 \text{ kg}^{-1} \text{ s}^{-2}$ is gravitational constant. Finally, we get R_{wing} with a median value of ten pc for both type 1 and type 2 subsamples. We stress that the value of R_{wing} we derive should be a lower limit since the region that the blue wing originates is not virialized.
2. **Physical mechanism.** In section 3.3, we find the wing component has a median of $V_{\text{off}}^{\text{wing}} = -162 (-97) \text{ km s}^{-1}$ for the type 1 (type 2) subsample. If we assume the velocity offset of wing

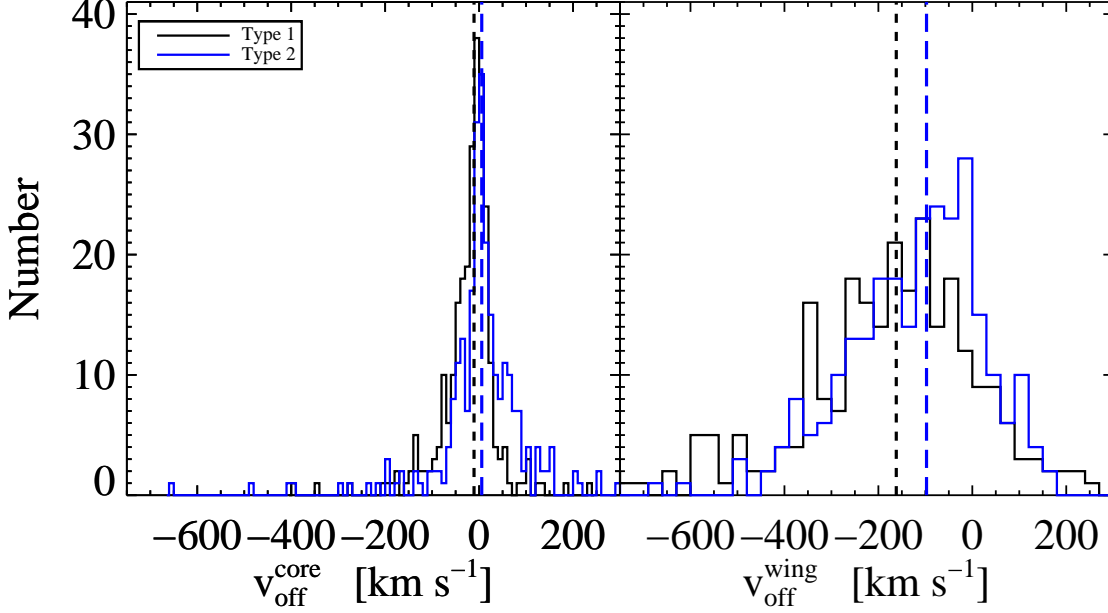


Fig. 6 Distributions of velocity offset relative to the system redshift for type 1 (*black*) and type 2 (*blue*) twin samples. The left panel for the core component, while the right panel for the wing component. The median values are marked by black vertical dash line for type 1s and blue vertical long dash line for type 2s.

component originates from the outflows which blow out in a direction perpendicular to the accretion disk, we would expect $V_{\text{off}}^{\text{wing}}(\text{type 2}) = V_{\text{off}}^{\text{wing}}(\text{type 1}) \times \cos \theta$, where θ is the opening angle of torus, $V_{\text{off}}^{\text{wing}}(\text{type 1})$ and $V_{\text{off}}^{\text{wing}}(\text{type 2})$ are median values of the velocity offset of the wing component for type 1 and type 2 AGNs, respectively. Applying $V_{\text{off}}^{\text{wing}}(\text{type 1}) = -162$ and $V_{\text{off}}^{\text{wing}}(\text{type 2}) = -97$, we get $\theta \sim 50^\circ$, this result is consistent with that from literatures (e.g., [Netzer 1987](#), [Krolik et al. 1994](#)).

In addition, we have not found any distinct correlation between $V_{\text{off}}^{\text{wing}}$ and galaxy properties (D4000, $\text{H}\delta_{\text{A}}$, stellar mass), as well as the physical properties of AGNs (bolometric luminosity, the Eddington ratio, black hole mass). The result is consistent with several previous studies (e.g., [Komossa et al. 2008](#); [Zhang et al. 2011](#)). If we accept a scenario in which the low-velocity gas in the core component is dominated by the gravity of the bulge, while the wing is more strongly influenced by the outflow cloud of active nucleus (e.g., [Zamanov et al. 2002](#); [Greene & Ho 2005](#)), the terminal outflow velocity would depend on the origin of the outflow on the one hand, and the deceleration mechanism on the other hand. [Komossa et al. \(2008\)](#) discussed several possibilities to explain the acceleration and entrainment of the NLR outflow, including radiation pressure, entrainment in radio jets, thermal winds, and high Eddington ratio. So the launching velocity of the outflow cloud is determined by different acceleration mechanisms and/or different stages of the AGN activity. Meanwhile, NLR outflow is de-

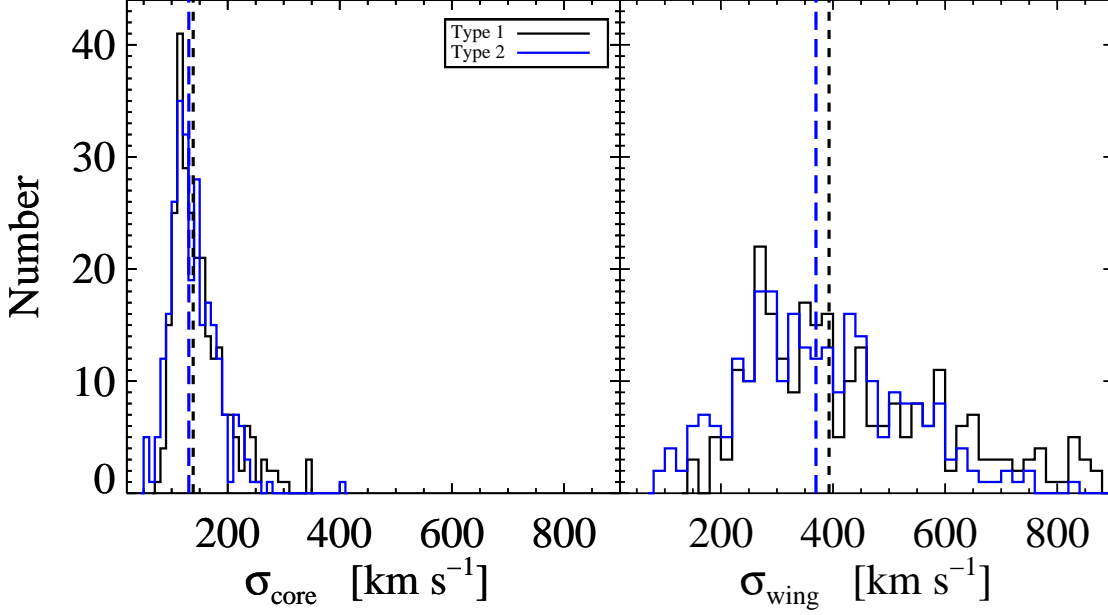


Fig. 7 Distributions of the line width σ for type 1 (*black*) and type 2 (*blue*) twin samples. The left panel for the core component, while the right panel for the wing component. The median values are marked by black vertical dash line for type 1s and blue vertical long dash line for type 2s.

celerated by the ISM of the host galaxy. Denser ISM results in more efficient deceleration, implying lower velocity (Zhang et al. 2011). Anyway, both accelerated mechanisms and the column density of NLR cloud would lead to different terminal velocities, thereby explaining the lack of correlation between the observed $V_{\text{off}}^{\text{wing}}$ and the physical properties of AGNs.

5 CONCLUSION

We select a type 2 AGN sample from SDSS DR7. In this sample, two Gaussian components are required to model the [O III] $\lambda 5007$ emission line, a broad wing plus a narrow core. We measure the velocity shift (relative to the absorption lines), line width and flux of both components. Combining our type 2 AGN sample with a type 1 sample from Zhang et al. (2011), we find that:

1. there is a tight correlation between the fluxes of wing and core components in both type 1 and type 2 samples. In both samples, the flux of the wing components is roughly equal to that of the core components.
2. in the unification scheme of AGNs, the type 1 and 2 AGNs are intrinsically the same, their different appearance is due to that we observe them from different direction, a dusty torus blocks the continuum source and broad-line region in type 2 AGNs. The difference in the velocity shift of the broad wing between type 1 and type 2 AGNs consists with a picture in which the broad wing originates

from outflows and the outflows blow out in a direction perpendicular to the accretion disk with a certain opening angle.

3. the velocity shift of the wing component has only weak, if any, correlations with the physical properties of AGNs (bolometric luminosity, the Eddington ratio and the mass of supermassive black holes) and the host galaxies (D4000, $H\delta_A$ or stellar mass). We suggest the lack of correlation is due to that the outflow is driven by both AGN and star formation activity. However, the contribution of AGN and star formation activity to the outflow varies from object to object. Future IFU survey like MaNGA (Mapping Nearby Galaxies at APO) will help us to understand, AGN and star formation, which is the primarily driver of outflow in a certain object.

Acknowledgements Zhixin Peng thanks Jing Wang for useful discussions. The research is supported by the National Natural Science Foundation of China (NSFC; Grant Nos. 11273015, 11133001 and 11003007), the National Basic Research Program (973 program No. 2013CB834905), and Specialized Research Fund for the Doctoral Program of Higher Education (20100091110009).

Funding for the creation and distribution of the SDSS Archive has been provided by the Alfred P. Sloan Foundation, the Participating Institutions, the National Aeronautics and Space Administration, the National Science Foundation, the US Department of Energy, the Japanese Monbukagakusho, and the Max Planck Society. The SDSS Web site is <http://www.sdss.org>.

The SDSS is managed by the Astrophysical Research Consortium (ARC) for the Participating Institutions. The Participating Institutions are The University of Chicago, Fermilab, the Institute for Advanced Study, the Japan Participation Group, The Johns Hopkins University, Los Alamos National Laboratory, the Max-Planck-Institute for Astronomy (MPIA), the Max-Planck-Institute for Astrophysics (MPA), New Mexico State University, University of Pittsburgh, Princeton University, the United States Naval Observatory and the University of Washington.

References

- Abazajian, K. N., Adelman-McCarthy, J. K., Agüeros, M. A., et al. 2009, *ApJS*, 182, 543 2
- Alexander, D. M., & Hickox, R. C. 2012, *New A Rev.*, 56, 93 2
- Aoki, K., Kawaguchi, T., & Ohta, K. 2005, *ApJ*, 618, 601 2
- Baldwin, J. A., Phillips, M. M., & Terlevich, R. 1981, *PASP*, 93, 5 2
- Bian, W., Yuan, Q., & Zhao, Y. 2005, *MNRAS*, 364, 187 2
- Boroson, T. 2005, *AJ*, 130, 381 2
- Brinchmann, J., Charlot, S., White, S. D. M., et al. 2004, *MNRAS*, 351, 1151 3
- Charlot, S., & Bruzual, G. 2013, *in preparation*, astrophysics Source Code Library 3
- Colbert, E. J. M., Baum, S. A., Gallimore, J. F., et al. 1996, *ApJS*, 105, 75 2
- Collin, S., Kawaguchi, T., Peterson, B. M., & Vestergaard, M. 2006, *A&A*, 456, 75 8
- Crenshaw, D. M., Schmitt, H. R., Kraemer, S. B., Mushotzky, R. F., & Dunn, J. P. 2010, *ApJ*, 708, 419 2
- Fabian, A. C. 1999, *MNRAS*, 308, L39 1
- Ferrarese, L., & Merritt, D. 2000, *ApJL*, 539, L9 1, 5
- Gebhardt, K., Bender, R., Bower, G., et al. 2000, *ApJL*, 539, L13 1, 5
- Greene, J. E., & Ho, L. C. 2005, *ApJ*, 630, 122 9
- Heckman, T. M., Miley, G. K., & Green, R. F. 1984, *ApJ*, 281, 525 2
- Heckman, T. M., Miley, G. K., van Breugel, W. J. M., & Butcher, H. R. 1981, *ApJ*, 247, 403 2
- Holt, J., Tadhunter, C. N., & Morganti, R. 2008, *MNRAS*, 387, 639 2
- Hopkins, P. F., Hernquist, L., Cox, T. J., et al. 2006, *ApJS*, 163, 1 1
- Kauffmann, G., & Heckman, T. M. 2009, *MNRAS*, 397, 135 5
- Kauffmann, G., Heckman, T. M., Tremonti, C., et al. 2003, *MNRAS*, 346, 1055 3
- Komossa, S., Xu, D., Zhou, H., Storchi-Bergmann, T., & Binette, L. 2008, *ApJ*, 680, 926 2, 6, 9
- Krolik, J. H., Madau, P., & Zycki, P. T. 1994, *ApJL*, 420, L57 9
- Lupton, R. 1993, *Statistics in theory and practice* 3

- Nelson, C. H., & Whittle, M. 1996, *ApJ*, 465, 96 [1](#)
- Netzer, H. 1987, *MNRAS*, 225, 55 [9](#)
- Silk, J., & Rees, M. J. 1998, *A&A*, 331, L1 [1](#)
- Stern, J., & Laor, A. 2013, *MNRAS*, 431, 836 [2](#)
- Tremaine, S., Gebhardt, K., Bender, R., et al. 2002, *ApJ*, 574, 740 [1](#), [5](#)
- Tremonti, C. A., Heckman, T. M., Kauffmann, G., et al. 2004, *ApJ*, 613, 898 [3](#)
- Whittle, M. 1992, *ApJS*, 79, 49 [1](#)
- Whittle, M., Pedlar, A., Meurs, E. J. A., et al. 1988, *ApJ*, 326, 125 [2](#)
- York, D. G., Adelman, J., Anderson, J. E., Jr., et al. 2000, *AJ*, 120, 1579 [2](#)
- Zamanov, R., Marziani, P., Sulentic, J. W., et al. 2002, *ApJL*, 576, L9 [2](#), [9](#)
- Zhang, K., Dong, X.-B., Wang, T.-G., & Gaskell, C. M. 2011, *ApJ*, 737, 71 [1](#), [2](#), [4](#), [5](#), [6](#), [7](#), [9](#), [10](#)
- Zhang, K., Wang, T., Dong, X., & Lu, H. 2008, *ApJL*, 685, L109 [2](#)
- Zhang, K., Wang, T.-G., Gaskell, C. M., & Dong, X.-B. 2013, *ApJ*, 762, 51 [2](#)